

Spin-orbit coupling in unoccupied quantum well states: Experiment and theory for Co/Cu(001)Cheng-Tien Chiang, Aimo Winkelmann, Ping Yu, Jürgen Kirschner, and Jürgen Henk
Max-Planck-Institut für Mikrostrukturphysik, Weinberg 2, D-06120 Halle (Saale), Germany

(Received 21 December 2009; revised manuscript received 9 February 2010; published 19 March 2010)

The influence of spin-orbit coupling in the unoccupied sp_z quantum well states in ultrathin Co films is investigated by two-photon photoemission spectroscopy with linearly polarized light. The asymmetry of the experimental two-photon photoemission intensities upon magnetization reversal is as large as 10%, which is in striking contrast to expectations based on the weakness of spin-orbit coupling in the observed quantum well states. The magnetic dichroic signal depends strongly on the polarization of the incident light as well as on the spin polarization of the quantum well states. These findings are explained by detailed electronic structure calculations and one-photon photoemission calculations. Our conclusions are supported by analytical considerations. In this way, a detailed picture of spin-orbit coupling in the unoccupied Co/Cu(001) quantum well states is provided.

DOI: [10.1103/PhysRevB.81.115130](https://doi.org/10.1103/PhysRevB.81.115130)

PACS number(s): 79.60.-i, 73.21.Fg, 71.70.Ej

I. INTRODUCTION

The coupling between spin and orbital angular momentum in the relativistic electronic structure is essential in the interplay between the electronic and lattice degrees of freedom with the electron spin in solid state systems, including their dynamical properties. In particular, the mechanism of spin-orbit coupling (SOC) can be exploited to provide access to the electron spin via purely optical excitation,¹ which is relevant in investigations of the relativistic band structure of nonmagnetic and magnetic solids by photoemission,^{2,3} in laser-based ultrafast magnetism,⁴ and in optically controlled spintronics.⁵ In a magnetic system, the optical transition rates between electronic states can be strongly influenced by the spin-orbit interaction. This leads to element-specific dichroism in optical absorption⁶ and photoemission^{7,8} and gives access to magnetic properties of materials without an experimentally more demanding external spin analysis.^{3,9} Powerful applications of magnetic dichroism include the element-specific imaging of magnetic domains in photoemission electron microscopy,¹⁰ the determination of spin and orbital magnetic moments and their anisotropy by core-level x-ray magnetic circular dichroism (XMCD),¹¹ and the study of the hybridization of occupied electronic states by angle-resolved photoemission spectroscopy (ARPES).^{2,12-14} Moreover, by exploiting the time resolution given by ultrashort laser pulses, magnetic dichroism can provide access also to the dynamics of spin and orbital angular momentum down to the femtosecond regime.^{15,16}

Since excited states naturally play a key role in optically driven processes, it is important to characterize to which degree these states are influenced by spin-orbit coupling. For this purpose, investigations of magnetic dichroism have to be extended to the unoccupied states with energies between the Fermi and the vacuum level. Inaccessible by conventional ARPES experiments based on one-photon photoemission (1PPE), these states can be approached by two-photon photoemission (2PPE) using lasers with photon energies in the order of a few electron volts.^{17,18} In such 2PPE experiments, magnetic linear¹⁹ and circular²⁰ dichroism were recently observed. In these investigations, however, the dichroic signal

was not related to specific unoccupied states. In another 2PPE investigation, we have demonstrated magnetic dichroism from unoccupied states for the well understood and characterized Co films on Cu(001).²¹ These experiments addressed the dispersion of unoccupied quantum well states in the Co film in connection with magnetic circular dichroism (MCD) and magnetic linear dichroism (MLD). The sizable MLD, with a maximum intensity asymmetry under magnetization reversal of about 10%, is particularly astonishing since it is common knowledge that MLD is large in band structure regions where electronic states hybridize strongly due to spin-orbit coupling; see, for example, Ref. 13 for Fe(110). The unoccupied Co quantum well states on Cu(001), however, are derived from the exchange-split sp_z bands²² which are thought to be negligibly affected by spin-orbit coupling but are found to show considerable MLD at energies far away from hybridization regions. Apparently, this finding questions the interpretation of magnetic dichroism studies performed so far. It thus seems necessary to establish whether the experimentally observed MLD can indeed be attributed to the unoccupied quantum well states. Because not only the unoccupied intermediate states but also the occupied initial states and the final outgoing photoelectron states are involved in the 2PPE process, we have to take into account the possible contributions from the occupied Co states²³ or even the final state²⁴ as origins of magnetic dichroism in the 2PPE experiments from Co/Cu(001). We will show that the established interpretation of MLD is still valid. In fact, we will demonstrate that MLD in 2PPE is a suitable tool for investigating even marginal hybridizations, which are mediated by spin-orbit coupling, provided an appropriate setup is chosen.

The above questions can hardly be answered by experiments alone. Thus, there is need for a joint experimental and theoretical investigation of Co/Cu(001) on which we report in this paper. The major issues to be addressed are: how large is the spin-orbit induced hybridization in the unoccupied Co quantum well states? If it is tiny, as expected, is it nevertheless large enough to produce the significant MLD found in experiment? How crucial is the choice of the setup, in particular the polarization of the excitation light and its incidence angle, for obtaining large asymmetries? A detailed pic-

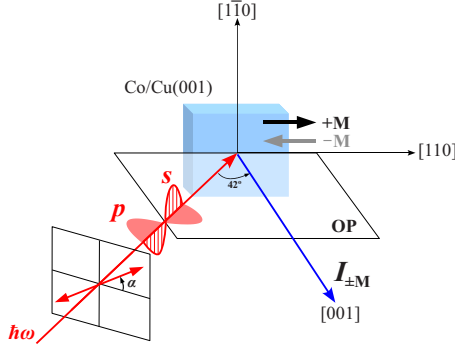


FIG. 1. (Color online) Setup for magnetic linear dichroism in 2PPE from Co/Cu(001). The 2PPE intensities $I_{\pm M}$ are detected in normal emission (blue arrow along [001]), with the in-plane magnetizations along [110] (+ M) or $[\bar{1}\bar{1}0]$ ($-M$). The optical plane (OP) is spanned by the surface normal and the incidence direction of the linearly polarized light (red arrow; polar angle 42°). The electric field vector (red double arrow) is rotated by an angle α out of the OP and can be tuned continuously between s and p polarization.

ture of the unoccupied quantum well states is obtained by relating results of 2PPE experiments, first-principles electronic structure calculations, 1PPE calculations, and analytical considerations.

The paper is organized as follows. Methodical aspects of both experiment and theory are addressed in Sec. II. Results are discussed in Sec. III, and conclusions are given in Sec. IV.

II. METHODOLOGICAL ASPECTS

A. Experimental

The experiments were performed at 300 K in an ultrahigh vacuum chamber with base pressure lower than 1×10^{-10} mbar. Ultrashort laser pulses with photon energy $\hbar\omega = 3.1$ eV served as the excitation light source for two-photon photoemission. The pulse width was about 20 fs, with an energy per pulse of about 1 nJ. The repetition rate was 81 MHz. The linear polarization of the incident light was controlled by an achromatic $\lambda/2$ waveplate, which tuned the electric field vector \mathbf{E} to any angle α with respect to the optical plane (Fig. 1). The latter is spanned by the incident direction (polar angle fixed to 42°) and the sample surface normal, parallel to a $(1\bar{1}0)$ plane containing the magnetic easy axis of the Co films. The photoelectrons were collected in normal emission by an electrostatic cylindrical sector energy analyzer (CSA 300, Focus GmbH). The energy resolution was about 100 meV, as was estimated from the vacuum cutoff at the low energy edge of the photoemission spectra.

Before growing the Co films, the Cu(001) substrate was cleaned by 2 keV Ar ion sputtering, followed by annealing up to 900 K in order to recover a smooth surface morphology. After cooling down to room temperature, the cleanliness and crystalline structure of the surface were confirmed by the clean Cu Auger electron spectrum and sharp low energy electron diffraction spots. Subsequently, Co films with a

thickness of several atomic layers were deposited on the well-prepared Cu(001) single crystal by an electron beam evaporator (EFM 3, Omicron) from a cobalt rod of 99.995% purity.

We measured 2PPE spectra continuously during film growth. The thickness-dependent intensity modulations with a period of one monolayer (ML) served as a self-calibrated indication of film thickness.²¹ Moreover, we observed the characteristic features of 2PPE through unoccupied quantum well states in the Co film and their evolution as a function of film thickness.²¹ For the magnetic dichroism measurements, the Co films are magnetized along the crystalline [110] (+ M) and $[\bar{1}\bar{1}0]$ ($-M$) directions by a magnetic field pulse generated from a copper coil (Fig. 1). 2PPE intensities $I_{\pm M}$ were then measured for $\pm M$.

B. Computational

The first-principles electronic structure calculations rely on the local spin-density approximation to density-functional theory. The computations were performed with our scalar-relativistic and fully relativistic multiple-scattering codes [Korringa-Kohn-Rostoker (KKR) (Ref. 25) and layer KKR (Ref. 26)], using the Perdew-Wang exchange-correlation functional.²⁷

The 1PPE calculations were performed with our relativistic layer-KKR code in which spin-orbit coupling and magnetism are treated on equal footing (Dirac equation). The spin-density matrix of the photoelectrons is computed within the relativistic one-step model of photoemission,^{26,28} using the potentials from the self-consistent electronic structure calculations as input. For photon energies in the optical region, as in this work, it is essential to include the dielectric response of the system by means of Fresnel's equations.

The systems comprise a semi-infinite face-centered cubic Cu(001) substrate, n monolayers of face-centered tetragonal Co layers ($n=1, \dots, 12$), and a semi-infinite vacuum region. The latter is modeled by so-called empty muffin-tin spheres. The Co films are assumed to continue epitaxially the Cu(001) substrate, with identical in-plane lattice constant (2.65 Å). A lattice contraction in perpendicular direction of 2% is assumed homogenous within the entire Co film, in reasonable agreement with crystallographic structure analyses (e.g., Refs. 29 and 30).

C. Setup and magnetic linear dichroism

Magnetic dichroism is the change in the photocurrent I upon reversal of the magnetization, $M \rightarrow -M$. It is quantified by the asymmetry A of the two intensities $I_{\pm M}$,

$$A \equiv \frac{I_{+M} - I_{-M}}{I_{+M} + I_{-M}}. \quad (1)$$

Our setup (Fig. 1) differs from the standard setup for MLD,³¹ in which the magnetization is normal to the optical plane and p -polarized light is commonly chosen. To observe MLD in the present setup, the electric field vector \mathbf{E} of the light has to be rotated out of the optical plane by an angle α : For $\alpha=0^\circ$ or $\pm 90^\circ$, one has p -polarized (\mathbf{E} within optical

plane) or s -polarized light (\mathbf{E} normal to optical plane), respectively: $\mathbf{E}(\alpha) = E_p \cos \alpha + E_s \sin \alpha$. In accordance with previous analytical and numerical considerations,³² there is no MLD for $\alpha = 0^\circ$ and $\pm 90^\circ$.

The present setup is rather similar to the standard setup for MCD in which the helicity vector and the magnetization are parallel or antiparallel (or are at least coplanar).³³ One might think that, because of the complex dielectric constant, the incident linearly polarized light produces elliptically polarized light in the sample and consequently the magnetic *linear* dichroism is close to magnetic *circular* dichroism. It has been shown theoretically for Ni(001), however, that this assumption does not hold.³² Experimental evidence is provided further by the different shapes of the asymmetries of MLD and MCD in 2PPE from Co/Cu(001); confer Fig. 3 in Ref. 21.

To analyze the dichroic intensities in more detail, the calculated electronic states are decomposed into the basis functions of the single-group representations Δ_i of the point group $4mm$ (C_{4v} in Schönflies notation; $i=1, 2, 2',$ and 5 ; $\Delta_{1'}$ contributions show up for f states³⁴ and are thus considered irrelevant in this work, which focuses on s , p , and d states). Due to the dipole selection rules, s -polarized light excites the Δ_5 part into the Δ_1 part of the electronic states, whereas p -polarized light excites both the Δ_1 and Δ_5 parts into the Δ_1 part.³⁵ According to the acknowledged picture,³¹ MLD is expected to be large for electronic states in which sizable Δ_1 and Δ_5 contributions are simultaneously present. We will show below that the Δ_1 and Δ_5 contributions hybridize only marginally in the unoccupied quantum well states of the Co films.

In two-photon photoemission, three types of electronic states are involved: the occupied initial state, the intermediate state, and the final state, all of which can in principle contribute to the magnetic dichroism. To pinpoint that the experimentally observed MLD is indeed due to the intermediate Co quantum well states we compare the experimental MLD in 2PPE with calculated MLD in 1PPE. On the one hand we consider 1PPE from the quantum well states into the same final state as in the 2PPE experiment, with photon energy $\hbar\omega = 3.1$ eV. Here, the quantum well states are assumed to be equally populated, which might not be true in 2PPE. With respect to these approximations we expect at least qualitative agreement of the theoretical 1PPE and the experimental 2PPE spectra. On the other hand we consider 1PPE from the occupied states of the 2PPE experiment into the final state, with photon energy $\hbar\omega = 6.2$ eV; thus the Co quantum well states are not involved in this process.

The comparison of experimental 2PPE and theoretical 1PPE motivated above assumes that 2PPE via an intermediate state (i.e., a quantum well state) can be treated as two independent sequential one-photon transitions: First, a one-photon transition from the initial state to the intermediate state and, second, one from the intermediate state to the final state. Within this approximation, the contribution in 2PPE that is solely due to the polarization from the coherent superposition of initial and final state is neglected; it does not involve the population of the intermediate state. Consequently, we are only concerned with the dichroic signal from the transition from the intermediate to the final state. As will

be shown in the following, this conveys information on spin-orbit coupling in the quantum well state and is in agreement with the experimental 2PPE results.

III. RESULTS AND DISCUSSION

A. Spin-orbit coupling in unoccupied Co quantum well states

First, we address the formation of the unoccupied quantum well states in Co films on Cu(001) (Fig. 2). These states are derived from the strongly dispersive and exchange-split sp_z bands of fct Co. Without spin-orbit coupling these belong at $\bar{\Gamma}$ (i. e. $k_{\parallel} = 0$) to the representation Δ_1 . They are confined on the vacuum side of the film by the image-potential barrier (surface barrier) and on the substrate side by a gap in the Δ_1 bands of the Cu band structure along Γ - Δ - X . Such a band gap shows up at energies higher than the maximum of the sp_z band, that is at $E > E_F + 1.63$ eV (horizontal arrow in Fig. 2). Consequently, majority quantum well states can exist from this energy up to the maximum of the Co majority sp_z band at $E_F + 2.85$ eV [dark gray area in Fig. 2(b)]. Likewise, minority quantum well states appear at energies up to $E_F + 3.04$ eV [light gray area in Fig. 2(b)].

In both the Cu and Co band structure, several band gaps appear as a consequence of the spin-orbit interaction.¹⁹ In particular if majority and minority states of Co hybridize, their spin-polarization changes sign (confer the bands turning from blue to red or vice versa in Fig. 2(b); note that spin is not a good quantum number due to spin-orbit coupling). The spin-orbit induced gaps appear mainly in the regime of the weakly dispersive d bands. In contrast, the strongly dispersive sp_z bands do not show any signature of spin-orbit coupling in the regions of the unoccupied quantum well states. Consequently, the associated Bloch states should be almost exclusively of Δ_1 character. That this is indeed the case is shown by displaying the relative weights of the single-group representations for each band (Fig. 3).

As addressed in Sec. II C, the relevant representations for the present photoemission setup are Δ_1 and Δ_5 whose weights are displayed in Figs. 3(a) and 3(b). The exchange-split sp_z bands hybridize with the minority Δ_5 band at about $E \approx 1.0$ eV and $k_{\perp} \approx 0.8(\Gamma$ - Δ - X) [this region is marked by circles in (a) and (b)]. As a result, a minority Δ_5 contribution is mixed into the sp_z states [Fig. 3(b)]; and, vice versa, Δ_1 contributions are mixed into the minority Δ_5 band [Fig. 3(a)]. Both additional contributions, however, decrease rapidly when leaving the hybridization region. To be more specific, the Δ_5 contribution to the sp_z bands is less than 1% in the regime of the quantum well states [gray areas in Fig. 3(b)]. We also performed a symmetry analysis of the Bloch spectral functions of the quantum well states in $\text{Co}_n/\text{Cu}(001)$; it fully confirms the picture derived from the bulk-band structure of fct Co, namely, that the quantum well states are marginally affected by hybridization and are almost of pure Δ_1 type.

Summarizing at this point, we find that the effect of spin-orbit coupling is very weak in the energy regime of the unoccupied Co sp_z quantum well states. Since hybridization due to the spin-orbit interaction is a prerequisite for MLD, this finding calls into question that the MLD observed in the

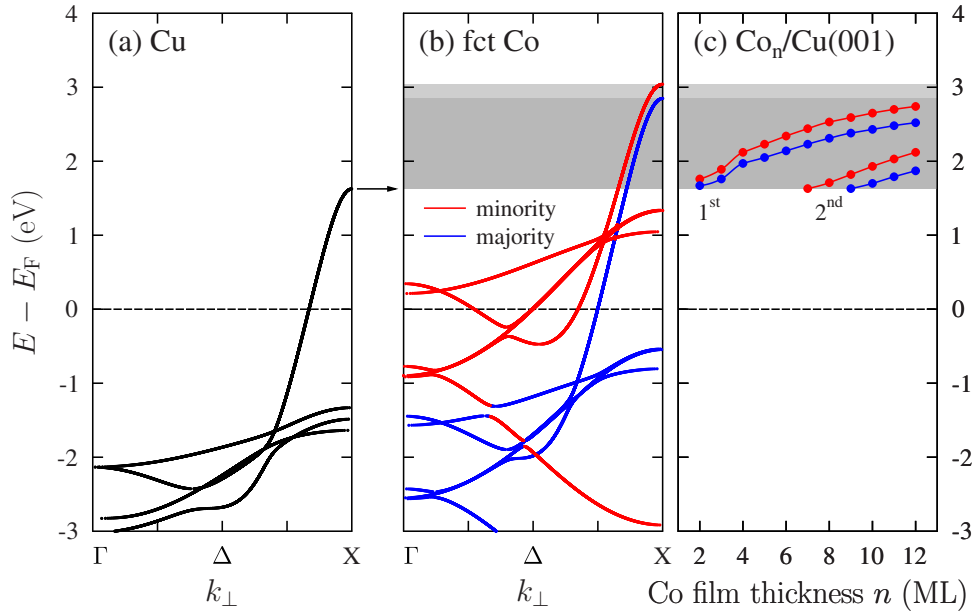


FIG. 2. (Color online) Formation of unoccupied quantum well states in Co/Cu(001). (a, b) Relativistic band structures of Cu (a) and fct Co (b) for the Γ - Δ -X direction. (c) Theoretical dispersion of unoccupied quantum well states in fct Co films on Cu(001) with thickness n from 2 to 12 ML. The two branches of states are labeled 1st and 2nd. The region in which unoccupied quantum well states can exist is highlighted by gray stripes in b and c. The horizontal arrow at the top of the Cu sp band marks the minimum energy for the unoccupied quantum well states. For Co, majority and minority spin orientations are indicated by blue and red symbols, respectively.

2PPE experiments can be attributed to the quantum well states.

B. Dispersion of the unoccupied Co quantum well states

To show that the exchange-split Co quantum well states are well described by the theory we address now their dispersion, that is the dependence of their energies on the Co film thickness n . The energy positions were obtained from

the maxima in the layer- and spin-resolved Bloch spectral function (Fig. 4).

A first set of bands is already present in the “window of quantum well states” [gray area in Fig. 2(c)] at 2 ML thickness (labeled “1st”). A parabolic dispersion, however, is obtained at thicknesses larger than about 3 to 4 ML, in agreement with experiment. A second set (“2nd”) shows up at 7 ML (minority spin) and 9 ML (majority spin), which is in agreement with experiment as well.²¹ Note that the exchange

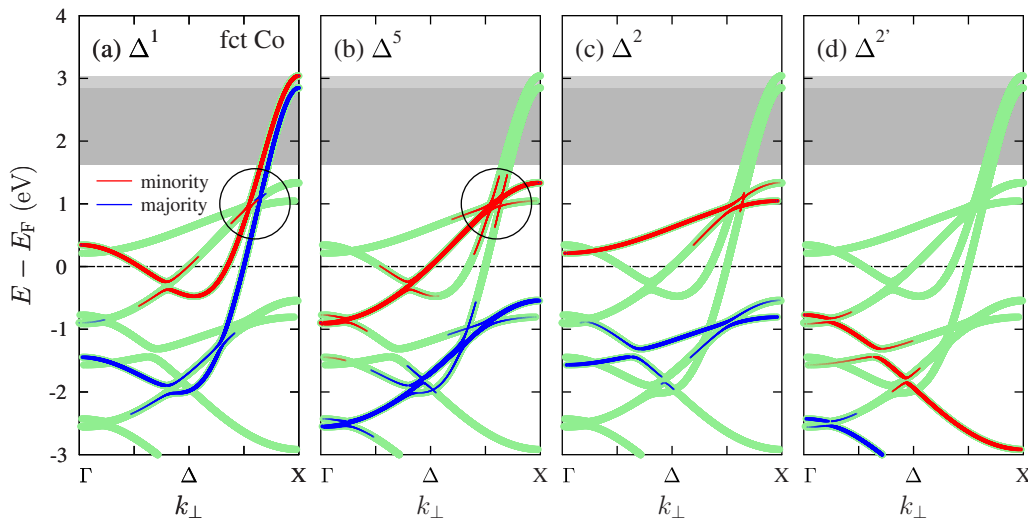


FIG. 3. (Color online) Relativistic band structure of fct Co along Γ - Δ -X, decomposed into representations Δ_1 (a), Δ_5 (b), Δ_2 (c), and Δ_2' (d) of the single-group 4 mm. Blue and red lines indicate majority and minority spin orientation, respectively. The line width is proportional to the relative weight of the representation of the associated Bloch state. The minimum weight shown is 1%. For clarity, the band structure itself is represented by green lines with fixed width. The region in which unoccupied quantum well states in fct Co/Cu(001) can exist is highlighted by gray stripes, as in Fig. 2(b). The circles in (a) and (b) guide to hybridization regions, which are discussed in the text.

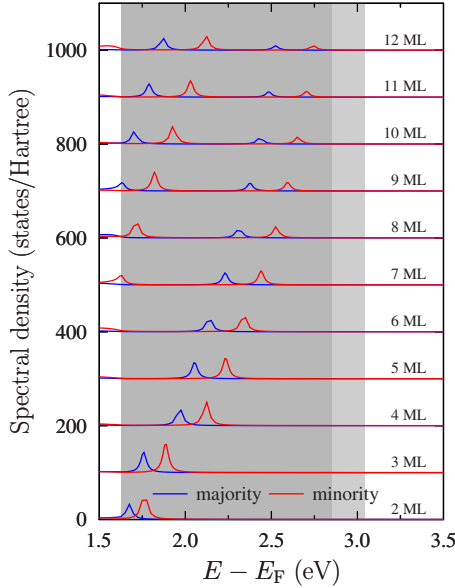


FIG. 4. (Color online) Bloch spectral function of the surface Co layer in $\text{Co}_n/\text{Cu}(001)$. Blue and red lines indicate majority and minority spin orientation, respectively. The Co film thickness n is given at the right of each data set; the spectra are offset vertically by 100 states/Hartree for clarity. The region in which unoccupied quantum well states can exist is highlighted by gray stripes, as in Fig. 2(b).

splitting increases with n . The dispersions for $n > 3$ ML can be well approximated by parabolae, indicating that the Co sp_z electrons can be regarded as nearly free.

The agreement between the theoretical dispersions and their experimental counterparts is addressed in Fig. 5. In our 2PPE experiments, electrons are selectively pumped into the

majority quantum well states, due to the majority character of the relevant initial states. This scheme is supported by the agreement of the experimental dispersion obtained from 2PPE and the calculated results for the first majority branch 1st in Fig. 5(a)]. The dispersions determined from spin-integrated inverse photoemission (Ortega *et al.*, Ref. 36) support our findings for the first branch. Spin-resolved inverse photoemission data (Yu *et al.*, Ref. 22) show also the second branches, which have higher energies than those in our calculations and, in particular for the thin Co films, lie outside the theoretically calculated region of quantum well states (confer the gray stripes in Fig. 2).

C. Magnetic linear dichroism in the unoccupied Co quantum well states

We now address the question whether the Δ_5 contribution, which is mixed into the Δ_1 quantum well states (Sec. III A), is sufficient to produce a significant MLD. It is important to stress that not only the weight of these contributions in the wave function is important but also the transition matrix elements; the latter enter explicitly the analytical expression for the photocurrent (Appendix).

Taking advantage of the dipole selection rules, we can disentangle the hybridized Δ_1 and Δ_5 components of the quantum well states by tilting the electric field vector \mathbf{E} of the incident light by an angle α out of the optical plane (cf. Sec. II C, Appendix, and Fig. 1). We have experimentally investigated the α -dependence of the quantum well states at film thicknesses 3.5 ML, 6 ML, and 16 ML; because all spectra show the same qualitative behavior we focus in the following on 6 ML as a representative (Fig. 6).

The experimental 2PPE intensities are maximum at $\alpha = 0^\circ$, that is for p -polarized light. Here, only the Δ_1 contri-

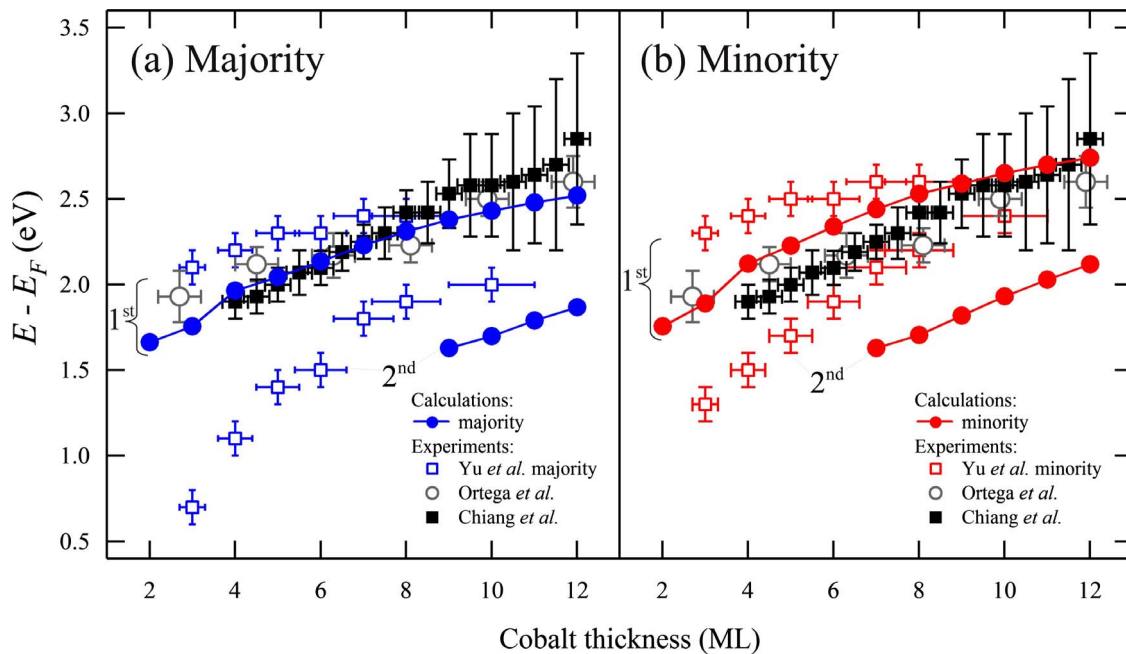


FIG. 5. (Color online) Dispersions of the unoccupied majority (a) and minority (b) quantum well states in $\text{Co}/\text{Cu}(001)$. Experimental data are extracted from inverse photoemission [Yu *et al.* (Ref. 22) and Ortega *et al.* (Ref. 36)] and 2PPE (Chiang *et al.*, Ref. 21). Theoretical data are taken from Fig. 2(c). The two sets of quantum well states are labeled by 1st and 2nd.

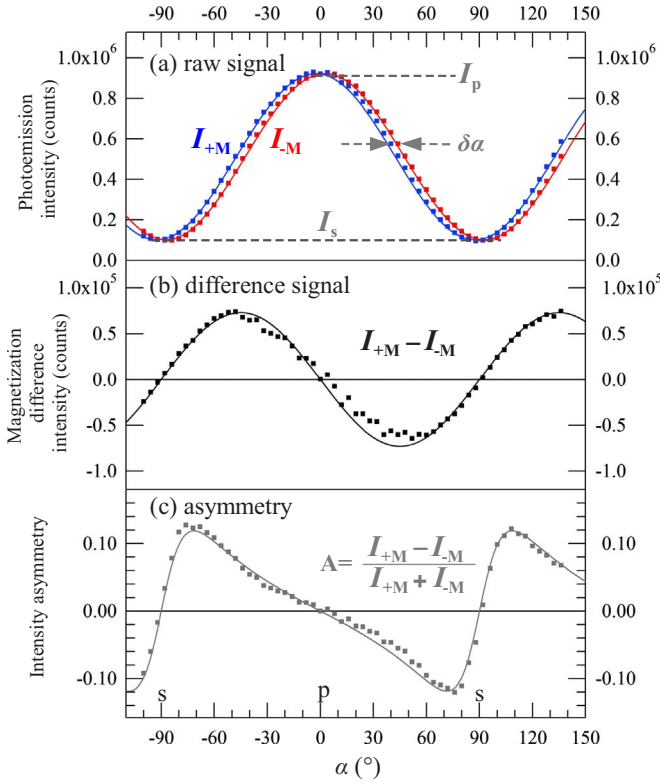


FIG. 6. (Color online) Magnetic linear dichroism in 2PPE experiments from the majority quantum well state in (6 ± 0.5) ML Co/Cu(001) with energy $E = E_F + (2.35 \pm 0.05)$ eV. The tilt angle α of the electric field vector of the incident light is defined in Fig. 1. (a) Photoemission intensities $I_{\pm M}$ for opposite magnetization directions $\pm M$ (Please note the corrected photoemission intensity compared to Fig. 4 in Ref. 21). (b and c) Difference $I_{+M} - I_{-M}$, and asymmetry derived from the raw intensities in (a). The photon energy $\hbar\omega$ is 3.1 eV. Solid lines display the α -dependence of the phenomenological model [cf. Appendix and Eq. (2)] with $\delta\alpha = 5^\circ$; I_s and I_p label the intensities for s - and p -polarized light [dashed lines in (a)].

bution to the quantum well state is probed. In contrast, the intensities are minimal for $\pm 90^\circ$ (s -polarized light) for which the Δ_5 contribution is probed. Neglecting for a moment matrix elements effects, this finding supports nicely the orbital character derived theoretically (Sec. III A): a strong Δ_1 but a weak Δ_5 contribution.

The intensities show a cosine dependence on the tilt angle α [Fig. 6(a)]. Further, the intensity difference $I_{+M} - I_{-M}$ is largest (in absolute value) at $\pm 45^\circ$ [Fig. 6(b)] whereas the asymmetry is largest at $\pm 75^\circ$ [Fig. 6(c)]. As will become clear from what follows, the position of the asymmetry extrema reflects the ratio of the dipole transition matrix elements that are related to excitations from the Δ_1 and the Δ_5 contributions of the quantum well state.

The α -dependence of the dichroic intensities is phenomenologically modeled as (Appendix)

$$I_{\pm M}(\alpha) = I_s \sin^2(\alpha \pm \delta\alpha/2) + I_p \cos^2(\alpha \pm \delta\alpha/2), \quad (2)$$

with I_s and I_p defined in Fig. 6(a). A fit to the experimental data gives $\delta\alpha = (5 \pm 1)^\circ$. The asymmetry defined in Eq. (1) can thus be approximated as

$$A(\alpha) = \frac{I_p - I_s}{2} \frac{\sin(2\alpha) \sin \delta\alpha}{I_s \sin^2 \alpha + I_p \cos^2 \alpha}. \quad (3)$$

The first term in the above expression determines mainly the amplitude of the asymmetry. The second term relates the tilt angle α_{\max} for which the asymmetry becomes extremal to the ratio of the intensities I_s and I_p for s and p polarization. Ignoring again the transition matrix elements, it reflects the Δ_5 and Δ_1 contributions to the quantum well state. From Sec. III A, we know already that the Δ_5 contribution (equivalent to a small I_s) is very small. Consequently, to obtain roughly similar weights of the two contributions, α_{\max} must be close to $\pm 90^\circ$, as is confirmed by its numerical values of $\pm 75^\circ$ (see also Appendix). This analysis supports the experimental value of $\delta\alpha$ of about 5° and rules out effects due to the magneto-optical Kerr effect since typical Kerr rotation angles are significantly smaller.

In the following, we provide theoretical evidence that the experimental findings are related to the unoccupied quantum well states and not to the occupied initial states. For this purpose, we calculated 1PPE spectra for which the quantum well states are assumed to be occupied, as is motivated in Sec. II C. The magnetic linear dichroism shows (in absolute value) largest numerical values at about $\alpha_{\max} = \pm 76^\circ$, with about 6% peak value [Fig. 7(c)]. The α dependence as well as the maximum asymmetry agree astonishingly well with those found in the 2PPE experiments (Fig. 6). Since occupied Co states are not involved in this 1PPE calculation, our finding corroborates that either the unoccupied Co quantum well states or, rather unlikely, the final states produce the sizable MLD.

The optical response of the system is taken into account by Fresnel's equations. With a dielectric constant $\epsilon = 1$, the linearly polarized light in the vacuum is transferred unaltered into the solid; with a complex dielectric constant ($\sqrt{\epsilon} = 1.61 + 3.05i$ for Co at $\hbar\omega = 3.0$ eV; Ref. 37), however, the incident light turns into a superposition of linearly and circularly polarized light within the solid. As a consequence, one observes in the former case a purely magnetic *linear* dichroism, whereas in the latter case one is concerned with superimposed *linear* and *circular* dichroisms.

Since the circular dichroism produces no α -dependence at all, the dependence on the tilt angle α can be solely ascribed to linear dichroism; this finding is evident from the asymmetries for $\epsilon \neq 1$ and $\epsilon = 1$ [Fig. 7(c)], which display identical shapes and, in particular, identical positions of the extrema. The asymmetry for $\epsilon \neq 1$ is, however, sizably larger than that for $\epsilon = 1$ [note the scale factor of 20 in Fig. 7(c)]. Thus, the *magnitude* of the effect is influenced by the additional circular dichroism introduced by the optical response, while the *position* of the asymmetry extrema is determined by the linear dichroism. This important effect of the optical response can be understood from Eq. (A2), where the two terms involving real and imaginary parts of $\sin \theta' E'_\parallel E'_\perp^*$ will correspond to purely linear (Re term) and circular dichroism (Im term) only in the limit of vanishing optical response ($\epsilon = 1$). With $\epsilon \neq 1$, both terms contribute to the magnetic dichroism.³²

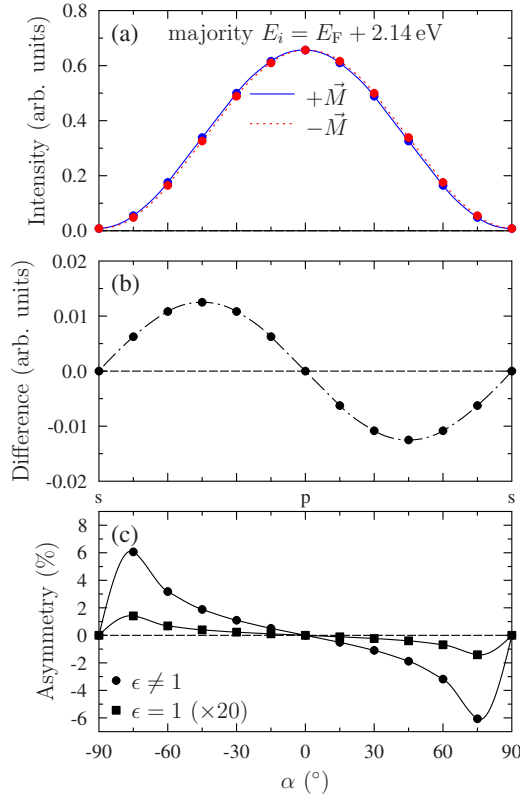


FIG. 7. (Color online) Theoretical magnetic linear dichroism in 1PPE from the unoccupied majority quantum well state in 6ML Co/Cu(001) with energy $E_F + 2.14$ eV (cf. Figure 2(c)). (a) Intensities $I_{\pm M}$ for magnetization direction $+M$ (blue, solid) and $-M$ (red, dotted) versus tilt angle α of the incident light. (b) Difference of $I_{\pm M}$. (c) Asymmetries derived from intensities that have been computed with optical response ($\epsilon \neq 1$; filled circles; shown in a) and without optical response ($\epsilon = 1$; filled squares, scaled by a factor of 20; intensities not shown). $\alpha = \pm 90^\circ$ correspond to s -polarized light, $\alpha = 0^\circ$ to p -polarized light. The photon energy $\hbar\omega$ is 3.1 eV.

These observations emphasize that the optical response is essential for quantitatively understanding the magnetic dichroism. We note in passing that the intensities from the minority quantum well state with energy $E_F + 2.35$ eV are very similar to those from the majority state. Its opposite spin polarization, however, manifests itself in an opposite sign of the asymmetry.

To rule out the final states of the photoemission process as origin of the magnetic linear dichroism we calculated 1PPE spectra for 6.2 eV photon energy, using the same final states as for $\hbar\omega = 3.1$ eV. Here, the unoccupied Co quantum well states are not involved but the occupied Co states serve as initial states. The theoretical spectra (not shown) reveal a cosine-dependence on α as well but an α_{\max} close to $\pm 45^\circ$ follows from almost equally large I_s and I_p . This finding clearly contrasts the experimental 2PPE observation. Assuming 2PPE as two sequential one-photon excitation processes, it supports that the Δ_1 and the Δ_5 parts of the quantum well states become probably equally populated in 2PPE by the initial excitation process; we note that the final state in photoemission (i.e., the photoelectron's wave function) belongs to the Δ_1 representation,³⁸ as do the unoccupied quantum

well states except for the tiny Δ_5 contribution mixed in by spin-orbit coupling. In conclusion, the agreement of the calculations for 1PPE from the unoccupied quantum well states and the disagreement of similar calculations from the occupied Co states with the 2PPE experiment, supports that the origin of the MLD in 2PPE are the unoccupied quantum well states.

IV. SUMMARY AND CONCLUSIONS

In summary, by relating results of 2PPE experiments, electronic structure and photoemission calculations, as well as analytical considerations, we have derived a more complete picture of the unoccupied quantum well states in Co films on Cu(001). The magnetic linear dichroism in 2PPE, here in a nonstandard setup, is found to be a valuable tool for the investigation of spin-orbit coupling in unoccupied states. Although the spin-orbit mediated hybridization is very weak, we showed that it can be clearly probed in 2PPE experiments when the excitation conditions are chosen properly.

Besides demonstrating the characterization of spin-orbit coupling in unoccupied states via magnetic linear dichroism in 2PPE, our results should be directly relevant for PEEM imaging of magnetization dynamics down to the fs-time scales provided by ultrashort laser pulses.^{39,40} In addition to the magnetization contrast provided by initial states near the Fermi level in threshold photoemission,^{41,42} the magnetic dichroism from the unoccupied Co quantum well states provides enhanced analytical potential because it is element-specific and it is sensitive to the film thickness.

ACKNOWLEDGMENTS

We gratefully acknowledge very fruitful discussions with A. Ernst and the technical support from F. Helbig.

APPENDIX: ANALYTICAL DESCRIPTION OF MAGNETIC LINEAR DICHROISM

In order to better understand the mechanism behind the observed dichroism, we use an analytical model, in addition to the numerical results presented in Sec. III C, to extract different contributions to the magnetic dichroism.

The electric field vector of the incident light is decomposed into components perpendicular to (subscript \perp) and within (subscript \parallel) the optical plane, respectively. The field inside the solid (quantities within the solid are marked by a prime) is given by Fresnel's formulas,

$$E'_{\perp} = 2E_0 \frac{\cos \theta \sin \alpha}{\cos \theta + \sqrt{\epsilon' - \sin^2 \theta}}, \quad (\text{A1a})$$

$$E'_{\parallel} = 2E_0 \frac{n' \cos \theta \cos \alpha}{\epsilon' \cos \theta + \sqrt{\epsilon' - \sin^2 \theta}}, \quad (\text{A1b})$$

where ϵ' is the complex dielectric constant and $n' = \sqrt{\epsilon'}$. θ and α are the polar angle of incidence and the tilt angle of the electric field vector with respect to the optical plane, respectively.

According to the analytical analysis of Ref. 32, the dichroic photoemission intensity can be written schematically as

$$\begin{aligned}
 I_{\pm M} = & (|E'_{\perp}|^2 + |\sin \theta'|^2 |E'_{\parallel}|^2) A_{(1,5)} + |\cos \theta'|^2 |E'_{\parallel}|^2 B_{(5)} \\
 & \pm 2 \operatorname{Re}(\sin \theta' E'_{\parallel} E'_{\perp}{}^*) \operatorname{Im} C_{(1,5)} \\
 & \pm 2 \operatorname{Im}(\sin \theta' E'_{\parallel} E'_{\perp}{}^*) \operatorname{Re} C_{(1,5)}. \quad (\text{A2})
 \end{aligned}$$

$A_{(1,5)}$ abbreviates an expression, which comprises terms of transition matrix elements for excitation from the Δ_1 and Δ_5 parts of the initial state; it is even under magnetization reversal. Likewise, the even $B_{(5)}$ is for excitations from the Δ_5 part. On the contrary, $C_{(1,5)}$ is odd under magnetization reversal; thus the magnetic linear dichroism is described by the last two terms in Eq. (A2), with an angular dependence given by $\sin \theta' E'_{\parallel} E'_{\perp}{}^*$ (Section II.C in Ref. 32; note that the subscript “(1,5)” reflects that hybridization among Δ_1 and Δ_5 parts is necessary for magnetic dichroism in our experimental geometry).

According to Snell’s law, $n' \sin \theta' = \sin \theta$ and $n' \cos \theta' = -\sqrt{\epsilon' - \sin^2 \theta}$, the internal polar angle θ' does not depend on the tilt angle α . Thus, the α -dependence of the dichroism is solely due to E'_{\perp} and E'_{\parallel} in $\sin \theta' E'_{\parallel} E'_{\perp}{}^*$, which with Eq. (A1) yields $\sin \alpha \cos \alpha$ or equivalently $\sin(2\alpha)/2$. Its maxima at $\alpha = \pm 45^\circ$ [orange and cyan in Fig. 8(a)] agree with the experimental and computational findings [Figs. 6(c) and 7(b)]. Consequently, we can condense Eq. (A2) further to

$$I = A \cos^2 \alpha + B \sin^2 \alpha \pm C \sin(2\alpha). \quad (\text{A3})$$

In contrast to the intensity difference, the experimental and theoretical asymmetries are maximum at about $\alpha = \pm 75^\circ$ [Fig. 6(d) and Fig. 7(c)], which is explained by the transition matrix elements. The emission from the Δ_1 part of the initial-state wave function, which is represented by A in Eq. (A3) is sizably stronger than that from the Δ_5 part, which is given by B in Eq. (A3), an argument that is supported by the group theoretical analysis given in Sec. III A. The experimental α -dependence is roughly reproduced by assuming $A \approx 9$, $B \approx 1$, and $C \approx 0.35$ [Fig. 8(b) and 8(c)]. Note that the dichroic intensities appear mutually shifted by a small angle $\delta\alpha$. Indeed, Eq. (A3) can be rewritten approximately as in Eq. (2),

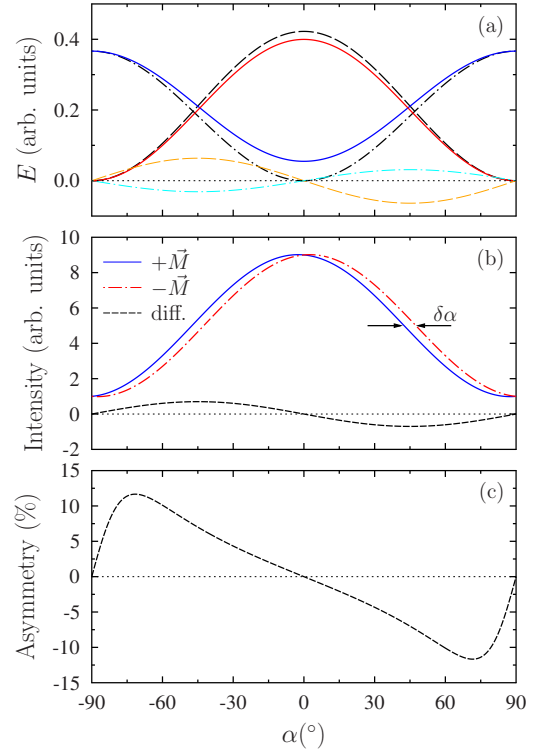


FIG. 8. (Color online) Analytical magnetic linear dichroism in 1PPE versus tilt angle α of the incident light. (a) Angular-dependent prefactors of the photoemission intensity Eq. (A2). Black: E'_{\perp} dash-dotted and E'_{\parallel} dashed, from eq. (a). Color: $|E'_{\perp}|^2 + |\sin \theta'|^2 |E'_{\parallel}|^2$ blue, $|\cos \theta'|^2 |E'_{\parallel}|^2$ red, $\operatorname{Re}(\sin \theta' E'_{\parallel} E'_{\perp}{}^*)$ orange dashed, and $\operatorname{Im}(\sin \theta' E'_{\parallel} E'_{\perp}{}^*)$ cyan dash-dotted. The photon energy, the dielectric constant of Co, and the polar angle of incidence are 3.1 eV, $\epsilon' = 1.61 + 3.05i$, and $\theta = 42^\circ$, respectively. (b) Photoemission intensities for $+M$ (blue) and $-M$ (red dash-dotted), calculated according to Eq. (A3). Their difference is shown as dashed line. The matrix element expressions that appear in Eq. (A3) are chosen to reproduce roughly the experimental results ($A/B/C = 9/1/0.35$). The angular shift $\delta\alpha = 5.5^\circ$ in Eq. (2) is indicated. (c) Asymmetry of the intensities shown in (b).

keeping terms up to first order in $\delta\alpha$. From Fig. 8(b), we obtain $\delta\alpha \approx 5.5^\circ$, which agrees nicely with the $(5 \pm 1)^\circ$ deduced from experiment.

¹M. Wöhlecke and G. Borstel, in *Optical Orientation*, edited by F. Meier and B. P. Zakharchenya (North-Holland, Amsterdam, 1984).
²W. Kuch and C. M. Schneider, Rep. Prog. Phys. **64**, 147 (2001).
³J. H. Dil, J. Phys.: Condens. Matter **40**, 403301 (2009).
⁴C. D. Stanciu, F. Hansteen, A. V. Kimel, A. Kirilyuk, A. Tsukamoto, A. Itoh, and T. Rasing, Phys. Rev. Lett. **99**, 047601 (2007).
⁵I. Žutić, J. Fabian, and S. Das Sarma, Rev. Mod. Phys. **76**, 323 (2004).
⁶G. Schütz, W. Wagner, W. Wilhelm, P. Kienle, R. Zeller, R.

Frahm, and G. Materlik, Phys. Rev. Lett. **58**, 737 (1987).

⁷L. Baumgarten, C. M. Schneider, H. Petersen, F. Schäfers, and J. Kirschner, Phys. Rev. Lett. **65**, 492 (1990).

⁸C. Roth, F. U. Hillebrecht, H. B. Rose, and E. Kisker, Phys. Rev. Lett. **70**, 3479 (1993).

⁹P. D. Johnson, Rep. Prog. Phys. **60**, 1217 (1997).

¹⁰C. M. Schneider, Z. Celinski, M. Neuber, C. Wilde, M. Grunze, K. Meinel, and J. Kirschner, J. Phys.: Condens. Matter **6**, 1177 (1994).

¹¹J. Stöhr, J. Magn. Magn. Mater. **200**, 470 (1999).

¹²A. Fanelsa, E. Kisker, J. Henk, and R. Feder, Phys. Rev. B **54**,

- 2922 (1996).
- ¹³A. Rampe, G. Güntherodt, D. Hartmann, J. Henk, T. Scheunemann, and R. Feder, *Phys. Rev. B* **57**, 14370 (1998).
- ¹⁴J. Bansmann, L. Lu, M. Getzlaff, M. Fluchtmann, J. Braun, and K. H. Meiwes-Broer, *J. Magn. Magn. Mater.* **185**, 94 (1998).
- ¹⁵C. Stamm, *et al.*, *Nature Mater.* **6**, 740 (2007).
- ¹⁶L. Braicovich and G. van der Laan, *Phys. Rev. B* **78**, 174421 (2008).
- ¹⁷M. Weinelt, *J. Phys.: Condens. Matter* **14**, R1099 (2002).
- ¹⁸H. Petek and S. Ogawa, *Prog. Surf. Sci.* **56**, 239 (1997).
- ¹⁹M. Pickel, A. B. Schmidt, F. Giesen, J. Braun, J. Minár, H. Ebert, M. Donath, and M. Weinelt, *Phys. Rev. Lett.* **101**, 066402 (2008).
- ²⁰K. Hild, J. Maul, G. Schönhense, H. J. Elmers, M. Amft, and P. M. Oppeneer, *Phys. Rev. Lett.* **102**, 057207 (2009).
- ²¹C.-T. Chiang, A. Winkelmann, P. Yu, and J. Kirschner, *Phys. Rev. Lett.* **103**, 077601 (2009).
- ²²D. H. Yu, M. Donath, J. Braun, and G. Rangelov, *Phys. Rev. B* **68**, 155415 (2003).
- ²³A. B. Schmidt, M. Pickel, T. Allmers, M. Budke, J. Braun, M. Weinelt, and M. Donath, *J. Phys. D* **41**, 164003 (2008).
- ²⁴X. Gao, A. N. Koveshnikov, R. H. Madjoe, R. L. Stockbauer, and R. L. Kurtz, *Phys. Rev. Lett.* **90**, 037603 (2003).
- ²⁵*Electron Scattering in Solid Matter*, edited by J. Zabloudil, R. Hammerling, L. Szunyogh, and P. Weinberger (Springer, Berlin, 2005).
- ²⁶J. Henk, in *Handbook of Thin Film Materials*, edited by H. S. Nalwa (Academic Press, San Diego, 2001), Vol. 2, Chap. 10, p. 479.
- ²⁷J. P. Perdew and Y. Wang, *Phys. Rev. B* **45**, 13244 (1992).
- ²⁸J. Braun, *Rep. Prog. Phys.* **59**, 1267 (1996).
- ²⁹E. Navas, P. Schuster, C. Schneider, J. Kirschner, A. Cebollada, C. Ocal, R. Miranda, J. Cerdá, and P. de Andrés, *J. Magn. Magn. Mater.* **121**, 65 (1993).
- ³⁰O. Heckmann, H. Magnan, P. le Fevre, D. Chandesris, and J. J. Rehr, *Surf. Sci.* **312**, 62 (1994).
- ³¹R. Feder and J. Henk, in *Spin-Orbit Influenced Spectroscopies of Magnetic Solids*, edited by H. Ebert and G. Schütz, Lecture Notes in Physics Vol. 466 (Springer, Berlin, 1996), p. 85.
- ³²J. Henk and R. Feder, *Phys. Rev. B* **55**, 11476 (1997).
- ³³W. Kuch, A. Dittschar, K. Meinel, M. Zharnikov, C. M. Schneider, J. Kirschner, J. Henk, and R. Feder, *Phys. Rev. B* **53**, 11621 (1996).
- ³⁴T. Inui, Y. Tanabe, and Y. Onodera, *Group Theory and Its Applications in Physics, Springer Series in Solid State Sciences* Vol. 78 (Springer, Berlin, 1990).
- ³⁵J. Henk, T. Scheunemann, S. V. Halilov, and R. Feder, *J. Phys.: Condens. Matter* **8**, 47 (1996).
- ³⁶J. E. Ortega, F. J. Himpsel, G. J. Mankey, and R. F. Willis, *Phys. Rev. B* **47**, 1540 (1993).
- ³⁷P. B. Johnson and R. W. Christy, *Phys. Rev. B* **9**, 5056 (1974).
- ³⁸J. Hermanson, *Solid State Commun.* **22**, 9 (1977).
- ³⁹C. M. Schneider and G. Schönhense, *Rep. Prog. Phys.* **65**, 1785 (2002).
- ⁴⁰T. Nakagawa, K. Watanabe, Y. Matsumoto, and T. Yokoyama, *J. Phys.: Condens. Matter* **21**, 314010 (2009).
- ⁴¹T. Nakagawa and T. Yokoyama, *Phys. Rev. Lett.* **96**, 237402 (2006).
- ⁴²T. Nakagawa, I. Yamamoto, Y. Takagi, K. Watanabe, Y. Matsumoto, and T. Yokoyama, *Phys. Rev. B* **79**, 172404 (2009).